U-Net and Active Contour Methods for Brain Tumour Segmentation and Visualization

Estera Kot
Faculty of Electrical Engineering
Warsaw University of Technology
Warsaw, Poland
kote@ee.pw.edu.pl

Zuzanna Krawczyk
Faculty of Electrical Engineering
Warsaw University of Technology
Warsaw, Poland
krawczyz@ee.pw.edu.pl

Krzysztof Siwek
Faculty of Electrical Engineering
Warsaw University of Technology
Warsaw, Poland
Krzysztof.Siwek@ee.pw.edu.pl

Piotr S. Czwarnowski
Nuclear Medicine Department
Medical University Of Warsaw
Warsaw, Poland
pczwarnowski@wum.edu.pl

***Abstract*—Gliomas are a type of brain and spinal tumour. They originate from glial cells that form the stroma of nerve tissue. Gliomas constitute about 70% of all intracranial tumours and are perceived as the leading cause of death due to brain tumours. This paper presents a comparison of three approaches for glioma detection, volume computation and 3D visualization. The classic approaches based on thresholding and active contour methods were compared with a deep learning implementation. The state-of-the-art model, named U-Net, was used to segment biomedical images which effectively removed bone images from computed tomography (CT) scans. To portion the tumour area, the Morphological Geodesic Active Contour method was applied. Model training was enriched by implementing a data augmentation strategy. Numerical results of tumour volume in cm3 were presented as well as a 3D visualization example.**

Keywords—Convolutional Neural Networks, U-Net, Brain Tumour, Glioblastoma, Active Contour, CT, PET

I. Introduction

Glioblastoma (GBM) are the most malicious primary brain tumours [1], with a 100% mortality rate and the fourth (the highest) histologic classification of the World Health Organization. The median lifetime for patients diagnosed with GBM is 14.6 months [2]. The objective of an established treatment plan is extending life expectancy and retaining quality of life and human functionality. In the Nuclear Medicine Department of the Medical University of Warsaw, at the Central Clinical Hospital, clinical trials are conducted using modern treatment plans for patients diagnosed with a glioblastoma. Following an examination, the standard medical procedure
is tumour extraction and introduction of a post-extraction radio and chemistry therapy plan. L– radiation emitter is injected into the area of the postoperative lodge, e.g. 213Bi.

Based on the CT and positron emission tomography (PET) scans, radiologists determine the amount of radiological substance, which simultaneously damages two strands of DNA. Radiologists and oncologists determine the volume of radiopharmaceutical inflicted, as well as the value of the probability of local cure TCP (Tumor Control Probability) based on microdosimetry methods, i.e. dosimetric measurements
for radiation exposure. Excess volume has the potential to damage healthy brain cells, and insufficient volume will fail to eradicate cancer cells. In order to increase the effectiveness of the introduced method and launch a replicable and error-proof approach with a precisely calculated tumour volume, its localization and shape are required.

The objective of this paper is to compare different methods to detect GBM, compute its volume and make a 3D visualization. The classical approach results of brain tumour segmentation were contrasted with a Convolutional Neural Networks (CNN) approach.

II. Literature Review

Automated segmentation of biological objects such as bone tissues or tumours is a challenging task due to high variability in the shape of such structures and unclear, blurred borders of the objects visible in medical data. Hence, the successful and accurate segmentation is still the subject of ongoing research.

Approaches to segmentation of bone structures out of medical data, presented in the literature, include inter alia, variety of active-contour based methods [3]-[5], thresholding operations and region growing methods [6]-[7], morphological methods as well as more elaborate atlas-based methods [8].

Analogously, the state-of-the-art algorithms of tumour segmentation cover region-based methods, i.e. the semi-automatic region growing algorithm described in [9] or watershed algorithm [10]. Another frequently used class of methods is the deformable contour approach [11]-[12].

Because of weak contrast between the tumour and healthy tissue, classical approaches often result in over-segmentation of the detected object. The accuracy of deformable contour or region growing method is also usually dependent on its correct initialisation by the user.

In recent years, the approach based on deep convolutional neural networks is becoming popular. The CNN application
to medical images allow to obtain promising results both in the area of segmentation of bone structures [13]-[14] as well as in tumour recognition task [15]-[18], and it gives hopes for better automation of the problem. However, what must be emphasised, to obtain satisfactory results, an extensive training set of expert-labelled data is needed.

978-1-7281-6926-2/20/$31.00 ©2020 IEEE

III. Dataset

A. Acquisition

The Nuclear Medicine Department delivered brain scans which were used during the development of algorithms. Images were taken using a Siemens Biograph 64 PET-CT scanner during the years 2016-2018. The brains of twenty-two male and female patients were tested. For each patient, 148 PET and 148 CT images were saved during a single examination. Additional examinations were performed on an undetermined number of patients.

CT scans present intracranial images of the soft tissues and structure of the brain surrounded by cerebrospinal fluid (CSF). GBM are nearly undetectable on CT scans. Therefore, PET scans are executed during a medical examination. The most accurate visualization of a tumour inside a brain utilises a fusion of CT and PET images from the same CT-PET scanner. The size of CT scans is 512x512 pixels. The structure of the brain
is reflected on CT scans as a level of grey, which indicates the degree of absorption of X-rays determined by Hounsfield units. The digital CT scan is represented in 12-16-bit greyscale (from 4096 to 65536 grey levels).

Fig. 1. is an example of a single slice from the received data. The software RadiAnt was used in the initial phase of the research to present CT, PET and CT-PET fusion scans. Uncompounded methods of marking tumour areas such as ellipse and line are shown on the right and left side of the figure.

Fig. 1. CT scan with corresponding PET scan. On the left side, there is a fusion of two brain images presented.

B. Data augmentation

Due to the small number of patient scans, to increase the size of the training dataset, data augmentation was applied. To train a robust CNN model, which realises image segmentation, a biomedical image augmentation strategy was developed. The objective of the written algorithm that implemented the U-Net model, was to remove bone tissue from CT images. A class named ImageDataGenerator from Keras library was utilised. A generator for both CT images and corresponding masks for each slide was implemented. Fig. 2. presents the results of artificially generated CT scans.

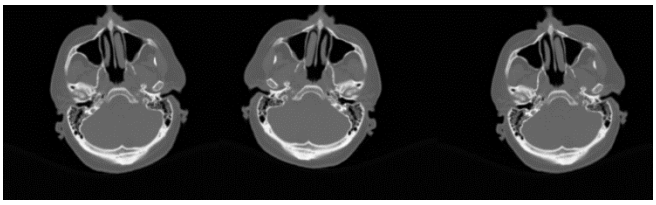

Fig. 2. Results from data augmentation strategy executed - transformed CT scans.

Elastic deformations were achieved with the practice of rotation, shear intensity, intervals, zooms and flip inputs horizontally. As a result, 13,480 files were generated. Fig. 3 shows the results of artificially generated masks for CT scans, that present bone tissues, the area where GBM do not occur.

Fig. 3. Results of data augmentation – three different masks which show skulls and bone structures.

IV. The Modern Method of Treatment of GBM

A. Glioblastoma traits

Glioblastoma multiforme can be characterized by infiltrated growth, intense migration and rapid spread of the tumour within the surrounding nerve tissue. The infiltration process occurs along nerve fibres, blood vessels, soft meninges and finally around nerve cells. This type of tumour growth prevents the complete surgical resection of glioma – hence tumour recurrences. However, gliomas generally have no metastatic capacity.

Both in the case of the tumour and the postoperative tumour bed, the tissues filling these volumes constitute the isotropic environment (none of the directions are therefore highlighted). The metabolism in tumour tissues is relatively slow (compared to the half-life) therefore it can be assumed that the results of the therapy depend on the effectiveness of radiation on these tissues not on the metabolism. Isotope radiotherapy is generally applied to patients with a GBM.

B. Methods of radiopharmaceutical administration

Radiopharmaceuticals were injected directly into the volume of the tumour or postoperative tumour bed – practically no internal irradiation of the patient, yet this method still requires surgical intervention (implantation of a catheter presented on the Fig. 4.).

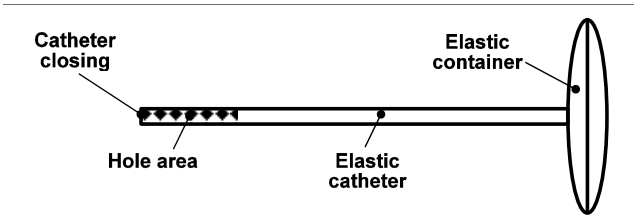

Fig. 4. Intracerebral administration in the method described above requires a flexible container-catheter set. The tank is flexible. The catheter is surgically inserted into the interior of the tumour or postoperative bed after tumour resection. The container remains outside the skull, just under the skin surface.

The reported activity of 213 Bi-DOTA-substance P [19] is about 2GBq combined with approximately 10MBq 68 Ga. As a result of the initial phase, the radiopharmaceutical fills the entire volume of the container-catheter set. It also emits alpha particles, which are primarily absorbed by the walls of the set.

The amount of radiopharmaceutical penetrating through the small holes in the walls of the catheter to the tissues of the tumour or postoperative bed is minimal. As a result of the controlled compression of the flexible container, the radiopharmaceutical fills the space between the catheter and the tissues of the tumour or postoperative bed. Subsequently, there is a significant increase in the contact area between the radiopharmaceutical and the tissues [20].

There is an overlap where the solution with a high concentration of radiopharmaceutical meets the tissue microstructure in which the radiopharmaceutical concentration is zero. This is the very beginning of a diffusion-like process using micro-circulation in tumour tissues. As a result of this process, isotope emitting alpha particles diffuse into the tumour and finally, the destruction of abnormal cancerous affected tissues.

The course of the procedure of controlled compression of the container-catheter set with radiopharmaceutical can have a significant impact on the effectiveness of therapy due to the pressure force and duration determining the shape of the contact surface of the solution containing the radiopharmaceutical with the surrounding tissues. Fig. 5 presents unsuccessful injection of the radiopharmaceutical.

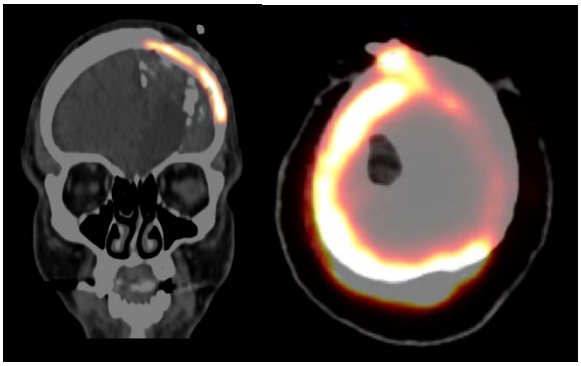

Fig. 5. Reflux resulting from a clogged catheter or too rapid administration of a radiopharmaceutical.

As a result, the rate at which the radiopharmaceutical is introduced into microcirculation in the tumour tissues changes. This rate is equal to the rate of administration of the isotope into the microcirculation and its further transport.

In isotopic radiotherapy, the therapeutic effects depend on the isotope, while the properties of radiopharmaceuticals are responsible for the transport of the isotope.

The emphasis on the container and its duration have a significant impact on the effectiveness of the presented therapeutic method. Optimization of these implements and factors from an effectiveness standpoint requires further research.

C. Expert's examination method

Thirty minutes after the isotope administration, a 5-minute acquisition is performed using a PET-CT TruePoint instrument with PETsyngo 6.7.3, VB42A from Siemens. In the PET image, the absorption reconstruction was performed based on CT.

Then, using TrueD software on a syngoMMWP VE40A, syngo VE32E workplace station from Siemens, the tumour tissue volume was measured where the radiopharmaceutical reached based on information from 68 Ga (B + decay).

Fig. 6. shows the result of an expert's examination – a glioma tumour is outlined.

Fig. 6. Result obtained by an expert.

Numerical results, obtained from the expert were presented in Table I, first column.

V. CLASSICAL APPROACH

A. Active Contours Methods

Classical methods such as local, global thresholding, CT and PET fusion, extracting bone tissue from PET and segmentation made by the usage of Active Contours methods (Edge and Chan-Vese) approach [21] was put in an application for brain tumour detection, volume computation and 3D visualization. Algorithms were developed in the MATLAB environment on a single CPU machine. Fig. 7. shows the exemplary process of removing bone tissue from a fusion of CT-PET scans.

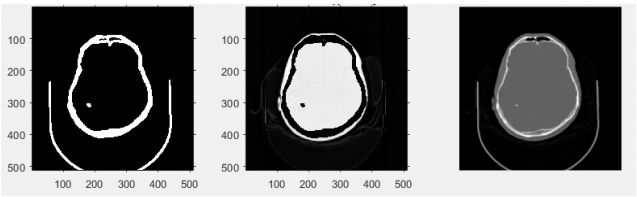

Fig. 7. Results from the initial phase of classical approach implementation. The left side of the figure presents a final binary image of a skull. In the middle there is visible a gray scale image with skull stripped away that is the input for the next phase of the algorithm – running active contour methods.

The most accurate results were obtained from the utilization of Edge Active Contour Method with 20 maximum iterations. For the Chan-Vese method, 100 iterations resulted in the closest volume in comparison with the expert's results. All numerical results of the calculated volumes of brain tumours in cm3 are presented in Table 1. For comparison, the brain size of the women participating in the studies was 1406.62 ± 101.41 cm3 at the age of 43.88 ± 14.74, and men 1406.57 ± 101, 69 cm3 at 42.96 ± 12.31 [22].

B. Phantom PET-CT

The phantom PET-CT was used to verify the algorithms described in the previous section. A phantom is a cylinder made of plexiglass (transparent plastic material). Inside the phantom, there are spheres of a known diameter that imitate tumours in the patient's body. The main purpose of the phantom is as an annual calibration of a medical apparatus aimed at controlling, maintaining and improving the quality of provided results. Each CT or PET scan is saved in DICOM format. It contains a parameter named "DateOfLastCalibration" that determine the time control since the last verification of the medical equipment. Fig. 8 shows the image of the used phantom.

Fig. 8. Phantom PET-CT produced by Biodex Medical Systems [23].

Radiotracer 168 Ga filled the spheres inside the phantom. The test was done on the same tomograph as the patient scans. Fifty-one CT scans and 51 PET images were obtained. Fig. 9. Is a representative of results with detected artificial tumours.

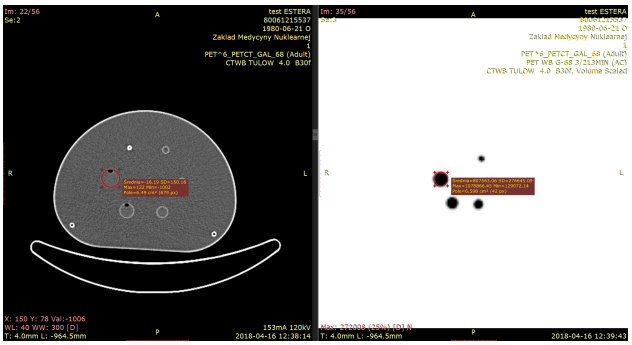

Fig. 9. Single slice for CT and PET scan for Phantom PET-CT.

Obtained scans were used to calibrate the developed algorithm and set the correct values for the global threshold. The final volume of simulated brain tumours was 21.41cm3. That was compared with the catalogue value for the phantom version. The percentage error between the two volumes was only 0.46%. Fig. 10. shows the intermediary result from the algorithm – detected tumours and their 2D contour.

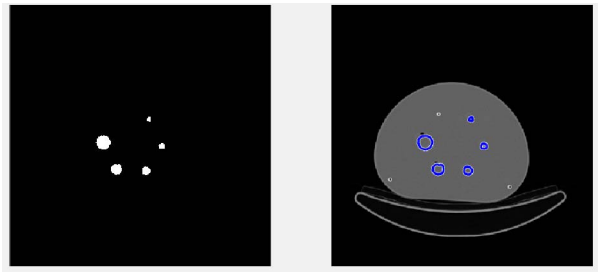

Fig. 10. On the left side, there are visible identified tumours on the PET image. On the right side, in the CT image, there are visible contours marking all tumours.

VI. The U-Net Approach

The U-Net is a Convolutional Neural Network (CNN) used mainly in the biomedical imaging area. The objective of image segmentation is to classify each pixel in the image belonging to the same class based on the pixel brightness. In the medical images that brightness is defined by the Hounsfield scale.

Designed by Olaf Ronneberger, Philipp Fischer and Thomas Brox in 2015, the U-Net objective is to process biological cell images [24]. In biomedical image cases, not only is classification preferrable – it is necessary for identification, typification and localization as well as measurement.

A. U-Net Architecture

The basic network foundation is presented on Fig. 11. U-Net does not follow a typical pattern for CNN which has fully connected layers.

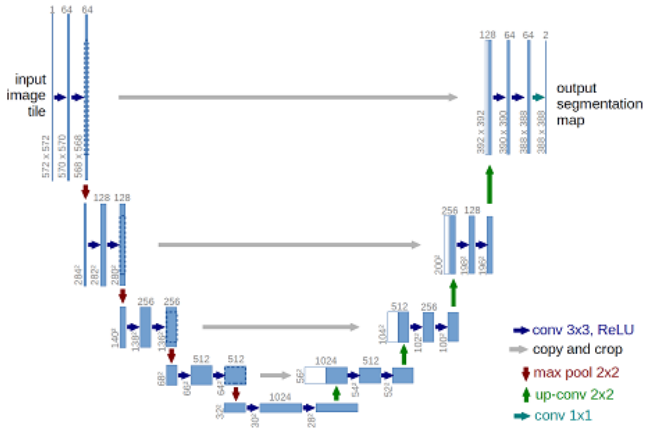

Fig. 11. U-net has a "U" shape symmetric architecture [24].

U-Net model is an example of an encoder-decoder scheme. The left side, named contracting path (also known as encoder), reduces the dimensionality of the inputs while maintaining appropriate data for the duty of interest (pooling). The right side, named an expansive path (also known as decoder), executes unsampling and attempts to recreate the input from the compressed image provided by the encoder.

B. Model Training

The U-Net model was utilised for bone tissue removal. The training part was achieved with scans labelled by the expert. From the total dataset, 20% of images were used for that phase.

The training objective is to decrease the differences between the grey levels of pixels (Hounsfield scale) and making the ROI of the areas labelled by the expert. The activation function was ReLU, excepting for the last layer where sigmoid activations were applied. The ADAM [25] optimiser and "Categorical Cross Entropy" as Loss Function were used. The model was trained in five epochs. Fig. 12. presents the results from the training – visible masks for bone tissues.

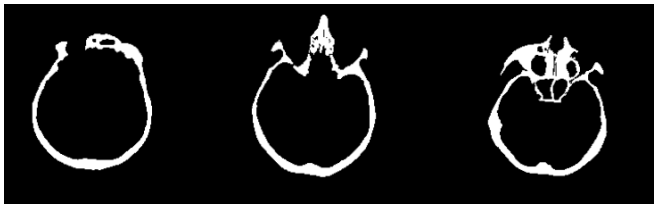

Fig. 12. Example of slides from CT scan, where U-Net segmented the bone tissues.

Due to the unpadded convolutions, the output image is smaller than the input by a constant border-width [20].

C. The design of the algorithm

Fig. 13 presents the conceptual diagram of the algorithm. Patient scans in DICOM format were structured by applying the naming convention and in catalogue formation. The U-Net produced masks of bone tissues that were subtracted from CT scans to eliminate the place where the GMB does not occur. Active Contour Method was run on each slice to outline the shape of the tumour. Volume computation was achieved from a baseline which was the area. The last phase was to make a 3D visualization of the achieved shape from 2D slices.

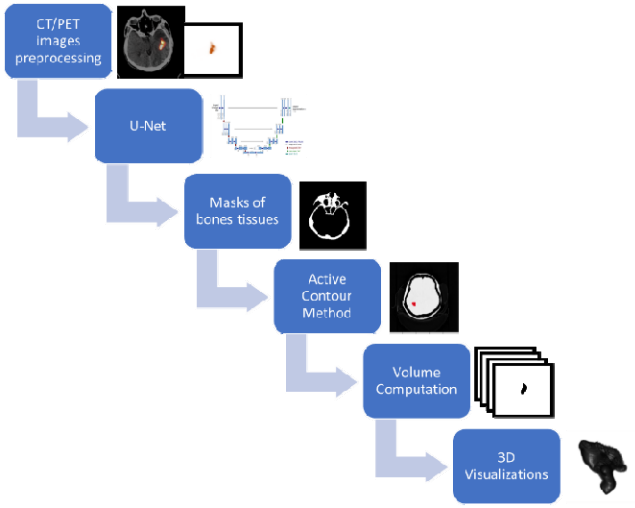

Fig. 13. The algorithm implementation was split to six phases. The images right to the description presents a demonstrative results from each step.

The algorithm with U-Net was developed using Python 3.7, Keras 2.3.1 and Tensorflow 2.0.0a0. The algorithm was trained and run on a single virtual machine with 64 virtual CPU(s), 259GiB of RAM. The best model achieved 97.39% accuracy and 7.76% loss – that give a comparable result to others that implement U-Net [26].

After the process of removing the bone tissues, Morphological Geodesic Active Contour method from Python's morphsnakes library was used to segment the tumour area. The behaviour of the utilised method is similar to that of Active Contours like Geodesic Active Contours [27].

VII. Computed Volumes Comparision

Table 1. presents results for seven patients obtained from the expert measurement of the classic approach implementation with two methods: Chan-Vese and Edge and with the modern approach – U-Net for bone tissues segmentation and Morphological Geodesic Active Contour for capturing the area of glioma. For patient number 6, the expert declined to measure the volume. For that patient's case, a too rapid injection of a radiopharmaceutical or a clogged catheter resulted in reflux.

TABLE I. TUMOUR VOLUMES [CM3]

L.p.	Expert	Active Contour		U-Net with active contour method
		Chan-Vese	*Edge*	
1.	17,11	17,37	38,18	13,76
2.	18,63	25,02	69,64	97,97
3.	30,22	11,13	19,35	29,26
4.	25,50	36,73	80,05	18,95
5.	13,32	12,79	27,24	11,92

L.p.	Expert	Active Contour		U-Net with active contour method
		Chan-Vese	*Edge*	
6.	-	7,76	12,67	7,82
7.	15,02	11,67	17,80	15,97

The U-Net model overestimation of tumour results can be caused by the small dataset used for training the net, noises left after the bone tissues extraction and utilizing less than optimal hyperparameters during training.

Table II presents 3D visualization for the same seven patients. Tumor 3D visualization was generated using an open source software, 3D Slice, due to the current version of algorithms operating on 2D images. The tumour shape, despite the used methods, remained the same or similar. Due to the typical characteristic of GBM, the shapes can be varied from a solid mass to fragmented and scattered small tumours.

TABLE II. TUMOUR 3D VISUALIZATION

Active Contour Chan-Vese	Active Contour Edge	U-Net with active contour method
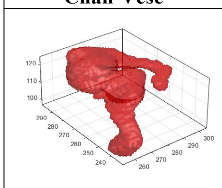	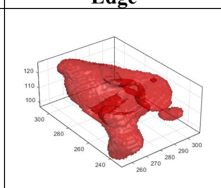	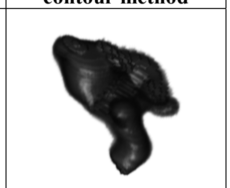
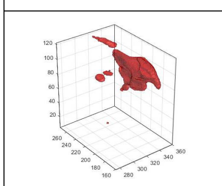	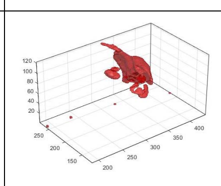	
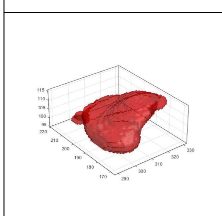	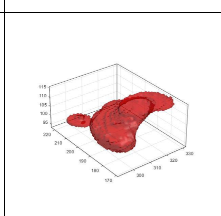	
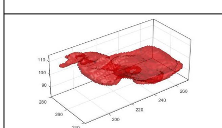	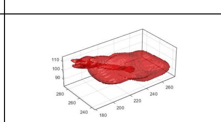	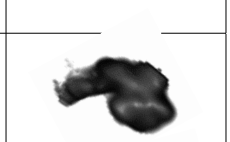
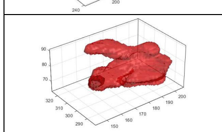	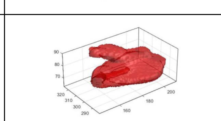	
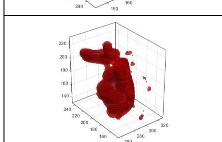	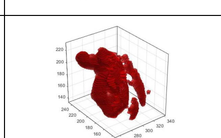	
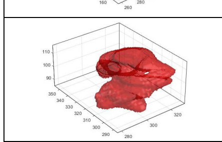	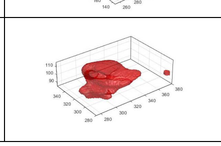	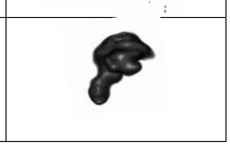

From a time computation perspective, the time needed for a single dataset to process both for U-Net and active contour is quite similar - around three (3) minutes for active contour and two (2) minutes for U-Net. However, U-Net required lengthy training hours making that approach significantly more time-consuming initially.

Our recommended improvements to the U-Net approach are to run the experiments using a pretrained U-Net and input alternate activation functions and optimizers. As for the training segment, there needs to be expanded experimentation with the number of batches and epochs as well as using morphological algorithms to remove the noise after the bone tissue segmentation process and before the Geodesic Active Contour Method. We do moreover acknowledge the value of the fusion of CT and PET scans running 3D U-Net as an effective approach to detecting the tumour without delays.

VIII. CONCLUSIONS

Brain tumour detection and volume computation is a prerequisite for the modern methods of GBM treatment which is developed in the Nuclear Medicine Department of the Medical University of Warsaw. In this paper, an approach for bone tissues segmentation via the usage of state-of-the-art model U-Net was proposed. With data augmentation strategy, an extensive dataset was produced, giving us an ability to train a model. The algorithm was developed which segmented the tumour from the post-U-net processed images. Achieved results were compared from three different approaches and two different environments. Applying active contours methods to detect tumours in biomedical images were proved as proper algorithms to obtain satisfactory numerical and visual outcomes.

Radiologists and Doctors of Medicine make the final decision regarding diagnoses. They often rely on the result of processing patient test results through hardware and software computer. For this reason, a key parameter required from algorithms in the field of medicine is precision and reliability. The problem that remains to be solved is the question of accurately determining the percentage of the entire tumour tissue volume that the radiopharmaceutical has reached. This operation should be performed on the fusion of positron emission tomography scans with magnetic resonance imaging (MRI) images.

REFERENCES

[1] A.F. Tamimi, M. Juweid, "Epidemiology and Outcome of Glioblastoma," In: De Vleeschouwer S, editor. Glioblastoma [Internet]. Brisbane (AU): Codon Publications; 2017 Sep 27. Chapter 8. Available from: https://www.ncbi.nlm.nih.gov/books/NBK470003/,DOI: 10.15586/codon.glioblastoma.2017.ch8.

[2] R. Stupp, WP Mason, MJ van den Bent,M Weller,B Fisher,MJ Taphoorn, et al., "Radiotherapy plus concomitant and adjuvant Temozolomide for glioblastoma," N Engl J Med. 2005;352:987–96.

[3] S. Li, X. Cui, N.C. June,H. Kim, K. Kwack,"Label-guided snake for bone segmentation and its application on Medical Rapid Prototyping,". IEEE International Conference on Systems, Man, and Cybernetics, 2011, 752-757.

[4] S. Ghadimi, H. Abrishami Moghaddam, R. Grebe and F. Wallois, "Skull Segmentation and Reconstruction From Newborn CT Images Using

Coupled Level Sets," in IEEE Journal of Biomedical and Health Informatics, vol. 20, no. 2, pp. 563-573, March 2016.

[5] PT Truc, TS Kim, S Lee, YK Lee, "A study on the feasibility of active contours on automatic CT bone segmentation," J Digit Imaging. 2010;23(6):793–805. doi:10.1007/s10278-009-9210-z.

[6] H. Aguirre-Ramos, J.G. Avina-Cervantes, I. Cruz-Aceves, "Automatic bone segmentation by a Gaussian modeled threshold," AIP Conference Proceedings. T. 1747. 2016. ISBN: 9780735414044. DOI: 10.1063/1.4954142.

[7] Y. Kang, K. Engelke, W.A. Kalender, "A new accurate and precise 3-D segmentation method for skeletal structures in volumetric CT data," in IEEE Transactions on Medical Imaging, vol. 22, no. 5, pp. 586-598, May 2003.doi: 10.1109/TMI.2003.812265.

[8] H. Lamecker, "A 3D statistical shape model of the pelvic bone for segmentation," W: Medical Imaging 2004: Image Processing. T. 5370. 2004, s. 1341. DOI: 10.1117/ 12.534145.

[9] Wu, Y.-P., Lin, Y.-S., Wu, W.-G., Yang, C., Gu, J.-Q., Bai, Y., & Wang, M.-Y. (2017) "Semiautomatic Segmentation of Glioma on Mobile Devices," Journal of Healthcare Engineering, 2017, 8054939. doi:10.1155/2017/8054939.

[10] M. Letteboer, et al., "Segmentation of tumors in magnetic resonance brain images using an interactive multiscale watershed algorithm1," Academic Radiology, Volume 11, Issue 10, 1125 – 1138.

[11] C. Dupont, N. Betrouni, N. Reyns, M. Vermandel, "On Image Segmentation Methods Applied to Glioblastoma: State of Art and New Trends," IRBM, Volume 37, Issue 3, 2016, Pages 131-143, ISSN 1959-0318, https://doi.org/10.1016/j.irbm.2015.12.004.

[12] C. Farmaki, K. Marias, V. Sakkalis, et al. "Spatially adaptive active contours: a semi-automatic tumor segmentation framework," Int J CARS 5, 369–384 (2010). https://doi.org/10.1007/s11548-010-0477-9.

[13] J. Minnema, M. van Eijnatten, W. Kouw, F. Diblen, A. Mendrik, J. Wolff, "CT image segmentation of bone for medical additive manufacturing using a convolutional neural network," Computers in Biology and Medicine, Volume 103, 2018, Pages 130-139, ISSN 0010-4825.

[14] J. Kleesiek, G. Urban, A. Hubert, D. Schwarz, K. Maier-Hein, M. Bendszus, A. Biller, "Deep MRI brain extraction: A 3D convolutional neural network for skull stripping," NeuroImage, Volume 129, 2016, Pages 460-469, ISSN 1053-8119.

[15] E. Lotan, R. Jain, N. Razavian, G.M. Fatterpekar, Y.W. Lui, "State of the Art: Machine Learning Applications in Glioma Imaging," American Journal of Roentgenology 2019 212:1, 26-37.

[16] G. Chlebus, A. Schenk, J.H. Moltz, "Automatic liver tumor segmentation in CT with fully convolutional neural networks and object-based postprocessing," Sci Rep 8, 15497 (2018). https://doi.org/10.1038/s41598-018-33860-7.

[17] M. Mittal, L. Goyal, S. Kaur, I. Kaur, A. Verma, D. Hemanth, "Deep learning based enhanced tumor segmentation approach for MR brain images," Applied Soft Computing, Volume 78, 2019, Pages 346-354, ISSN 1568-4946.

[18] M. Havaei, "Brain Tumor Segmentation with Deep Neural Networks," MedicalImage Analysis 35 (2017): 18–31. Crossref. Web.

[19] Cordier, D., Forrer, F., Bruchertseifer, F. et al. Eur J Nucl Med Mol Imaging (2010) 37: 1335. https://doi.org/10.1007/s00259-010-1385-5.

[20] P. Czwarnowski: "Wpływ rekonstrukcji na wartość SUV w padaniu PET-CT, " Fizyk Inżynier Medyczny, vol. 8, 1/2019, 38-39.

[21] E. Kot, K. Siwek, "Segmentation of brain biomedical images to compute the volume of gliomas," ITM Web of Conferences, 2019, 28.01016. 10.1051/itmconf/20192801016.

[22] E. Luders, A.W. Toga, P. M. Thompson, "Why size matters: differences in brain volume account for apparent sex differences in callosal anatomy: the sexual dimorphism of the corpus callosum," Neuroimage, 2013, pp. 84:820-4.

[23] Phantom PET-CT, Available from website: https://mediso.pl/img/27%20Fantomy%20PET%20i%20PET-CT.pdf.

[24] O. Ronneberger, P. Fischer, T. Brox, "U-Net: Convolutional Networks for Biomedical Image Segmentation", University of Freiburg, 2015.

[25] D. Kingma, J. Ba, "Adam: A method for stochastic optimization," CoRR, 2014.

[26] S. Humera, K. Shyamala, K., Z. Raniah, "Automatic Lung Segmentation on Thoracic CT Scans Using U-Net Convolutional Network," 2018, 0643-0647. 10.1109/ICCSP.2018.8524484.

[27] V. Caselles, R. Kimmel, G. Sapiro. "Geodesic Active Contours", In International Journal of Computer Vision (IJCV), 1997, DOI:10.1023/A:1007979827043.